J. Fluid Mech. (2001), *vol.* 426, *pp.* 135–154. Printed in the United Kingdom

Energy paths in edge waves

By C. J. CHAPMAN

Department of Mathematics, University of Keele, Keele, Staffordshire, ST5 5BG, UK

(Received 14 February 2000 and in revised form 24 July 2000)

In this paper the energy streamlines, energy paths, and energy streak lines in a steady or unsteady inhomogeneous acoustic field next to an unstable oscillating boundary, such as a vortex sheet or shear layer, are determined. The theory in the paper applies also to an evanescent wave produced by total internal reflection, and to any other type of edge wave, e.g. a coastally or topographically trapped wave in geophysical fluid dynamics. The idea of the paper is that energy velocity, i.e. energy flux divided by energy density, is defined at every point in space and time, not merely when averaged over a cycle. Integration of the ordinary differential equation for energy velocity as a function of position and time gives the energy paths. These paths are calculated explicitly, and are found to have starting and finishing directions very different from those of cycle-averaged paths. The paper discusses the physical significance of averaged and non-averaged energy paths, especially in relation to causality. Many energy paths have cusps, at which the energy velocity is instantaneously zero. The domain of influence of an arbitrary point on the boundary of a steady acoustic edge wave is shown to lie within 45° of a certain direction, in agreement with a known result on shear-layer instability in compressible flow. The results are consistent with flow visualization photographs of near-field jet noise. The method of the paper determines domains of influence and causality in any wave problem with an explicit solution, for example as represented by a Fourier integral.

1. Introduction

A method often used to introduce the idea of the energy velocity of a wave is to define this velocity as the ratio

$$\frac{\text{energy flux transmitted by the wave}}{\text{energy density of the wave}}. \tag{1.1}$$

The ratio is then shown to be equal to the group velocity $\partial\omega/\partial\boldsymbol{k}$ of the wave, i.e. the gradient of the wave frequency ω with respect to the wave vector $\boldsymbol{k}$, where ω is related to $\boldsymbol{k}$ by the dispersion relation of the wave. The method has been used by Lighthill (1960, equations A4, A15; 1965, equations 82, 87; 1978, p. 257; 1981, pp. 185, 189); by writers on general wave theory (Buchen 1971; Hayes 1977, 1980; Boulanger & Hayes 1993, pp. 158–159; Scott 1995); and, especially, by workers in geophysical fluid dynamics (e.g. Longuet-Higgins 1964; Buchwald 1972; Luyten 1973; Thomson 1973; Noda 1986; Gill 1982, pp. 141, 267, 502; Pedlosky 1987, pp. 121–122, 373–374). In all this work, the energy flux and energy density are first averaged over a wave cycle, so that energy flow on the scale of a wavelength and period is not described. On the other hand, (1.1) is equally valid without averaging, and it then determines energy velocity at every point in space and time. It may thus be used to determine the 'fine-scale' energy flow, and not merely the simpler 'cycle-averaged' energy flow.

We shall indicate differentiation with respect to time by a dot. Then if the value of (1.1) at an arbitrary position $\boldsymbol{x}$ and time t is denoted $\boldsymbol{U}(\boldsymbol{x}, t)$, the energy paths are the solutions $\boldsymbol{x}(t)$ of the ordinary differential equations

$$\dot{\boldsymbol{x}} = \boldsymbol{U}(\boldsymbol{x}, t). \tag{1.2}$$

We may think of these solutions $\boldsymbol{x}(t)$ as representing the motion of 'energy particles' – just as, if $\boldsymbol{U}$ represented fluid velocity instead of energy velocity, the solutions would represent the motion of 'fluid particles'. Such energy particles are fictitious, but perhaps no more so than fluid particles. Indeed, from a molecular point of view the macroscopic fluid velocity $\boldsymbol{u}(\boldsymbol{x}, t)$ is defined as the ratio of mass flux to mass density, analogously to (1.1), and the motion of a fluid particle is defined by a solution $\boldsymbol{x}(t)$ of $\dot{\boldsymbol{x}} = \boldsymbol{u}(\boldsymbol{x}, t)$. Thus in problems of energy transfer by waves, it seems legitimate to take (1.1)–(1.2) as a starting point and determine in detail the energy paths.

The positions at a fixed time t_1 of all the energy particles which passed through the point $\boldsymbol{x}_0$ at any earlier time form the energy streak line at t_1 from $\boldsymbol{x}_0$. We may also consider at time t_1 the 'frozen' equations

$$\dot{\boldsymbol{x}} = \boldsymbol{U}(\boldsymbol{x}, t_1). \tag{1.3}$$

The solutions $\boldsymbol{x}(t)$ of these equations form the energy streamlines at time t_1. In this paper the energy streamlines, energy paths, and energy streak lines in an acoustic edge wave (also called an evanescent wave, or an inhomogeneous wave, or a subsonic wave) are determined. The wave may be steady or unsteady. The method applies equally to any wave for which the energy flux can be unambiguously defined at a point, as appears always to be the case for waves in fluids. The method would not apply to electromagnetic waves, because the Poynting vector, a measure of energy flux at a point, is ambiguous to the extent of an arbitrary solenoidal field, which does not alter the total energy flowing out of a closed region. For waves in fluids, a comparable ambiguity has sometimes appeared to be present, especially in problems of geophysical fluid dynamics, but the ambiguity has later been removed by careful determination of which energy fluxes are associated with the wave (e.g. Gill 1982, p. 502; Pedlosky 1987, pp. 373–374).

We analyse unsteady edge waves in § 2 and steady edge waves in § 3. The physical significance of energy paths is discussed in § 4.

2. Unsteady edge waves

2.1. *Pressure field; dispersion relation*

We consider a sound wave in which the acoustic pressure p is of the form

$$p = p_0 \mathrm{e}^{\mathrm{i}(\boldsymbol{k}\cdot\boldsymbol{x} - \omega t)}. \tag{2.1}$$

The amplitude p_0 is assumed small enough for p to satisfy the wave equation. The speed of sound will be denoted c_0, so that $\boldsymbol{k}$ and ω satisfy the dispersion relation

$$\omega^2 = c_0^2 \boldsymbol{k}\cdot\boldsymbol{k}. \tag{2.2}$$

To represent an edge wave, we allow $\boldsymbol{k}$ and ω to be complex. Denoting real parts by a subscript r, and imaginary parts by a subscript i, we put

$$\boldsymbol{k} = \boldsymbol{k}_\mathrm{r} + \mathrm{i}\boldsymbol{k}_\mathrm{i}, \quad \omega = \omega_\mathrm{r} + \mathrm{i}\omega_\mathrm{i}. \tag{2.3}$$

Then the dispersion relation (2.2) is

$$\omega_r^2 - \omega_i^2 = c_0^2(\boldsymbol{k}_r \cdot \boldsymbol{k}_r - \boldsymbol{k}_i \cdot \boldsymbol{k}_i), \quad \omega_r \omega_i = c_0^2 \boldsymbol{k}_r \cdot \boldsymbol{k}_i. \tag{2.4}$$

When $\omega_i = 0$, the wave is steady; otherwise it is unsteady. In calculations for unsteady waves, it is convenient to use the slowness s_0 and the slowness vector $\boldsymbol{s}$ defined by

$$s_0 = 1/c_0, \qquad \boldsymbol{s} = \boldsymbol{k}/\omega. \tag{2.5}$$

Then the dispersion relation is

$$s_0^2 = \boldsymbol{s} \cdot \boldsymbol{s}. \tag{2.6}$$

We put

$$\boldsymbol{s} = \boldsymbol{s}_r + \mathrm{i}\boldsymbol{s}_i, \qquad s_r = |\boldsymbol{s}_r|, \qquad s_i = |\boldsymbol{s}_i|, \tag{2.7}$$

to obtain

$$s_0^2 = s_r^2 - s_i^2, \qquad \boldsymbol{s}_r \cdot \boldsymbol{s}_i = 0. \tag{2.8}$$

Thus $\boldsymbol{s}_r$ and $\boldsymbol{s}_i$ are perpendicular, and $s_r > s_i$. The relations (2.8) are used repeatedly in the calculations below. We define $\omega_0 > 0$ by

$$\omega_0^2 = \omega_r^2 + \omega_i^2. \tag{2.9}$$

Simple consequences of the above definitions are

$$\boldsymbol{s}_r = (\boldsymbol{k}/\omega)_r = (\omega_r \boldsymbol{k}_r + \omega_i \boldsymbol{k}_i)/\omega_0^2, \qquad \boldsymbol{s}_i = (\boldsymbol{k}/\omega)_i = (-\omega_i \boldsymbol{k}_r + \omega_r \boldsymbol{k}_i)/\omega_0^2, \tag{2.10a,b}$$

$$\boldsymbol{k}_r = \omega_r \boldsymbol{s}_r - \omega_i \boldsymbol{s}_i, \qquad \boldsymbol{k}_i = \omega_i \boldsymbol{s}_r + \omega_r \boldsymbol{s}_i. \tag{2.10c}$$

In (2.1) let us define

$$\theta = \theta(\boldsymbol{x}, t) = \boldsymbol{k} \cdot \boldsymbol{x} - \omega t. \tag{2.11}$$

Since $\boldsymbol{x}$ and t are real, we have $\theta = \theta_r + \mathrm{i}\theta_i$ where

$$\theta_r = \theta_r(\boldsymbol{x}, t) = \boldsymbol{k}_r \cdot \boldsymbol{x} - \omega_r t, \qquad \theta_i = \theta_i(\boldsymbol{x}, t) = \boldsymbol{k}_i \cdot \boldsymbol{x} - \omega_i t. \tag{2.12a,b}$$

Therefore $p = p_0 \mathrm{e}^{-\theta_i} \mathrm{e}^{\mathrm{i}\theta_r}$, with real part

$$p_r = p_0 \mathrm{e}^{-\theta_i} \cos\theta_r. \tag{2.13}$$

Typical contours of p_r at a fixed time are shown in figure 1(*a*). Since $\boldsymbol{s}_r$ and $\boldsymbol{s}_i$ are perpendicular, we shall use a coordinate system for $\boldsymbol{x}$ in which the $\boldsymbol{s}_r$-direction, drawn horizontally to the right, is the x_r-direction, and the $\boldsymbol{s}_i$-direction, drawn vertically upwards, is the x_i-direction. (The notation x_r, x_i is convenient, though somewhat illogical, because $\boldsymbol{x}$ is real; we make no use of 'complex position' or 'complex rays'.) Equations (2.8)–(2.12) give

$$\theta_r = \omega_r s_r (x_r - t/s_r) - \omega_i s_i x_i, \qquad \theta_i = \omega_i s_r (x_r - t/s_r) + \omega_r s_i x_i. \tag{2.14a,b}$$

Therefore in our coordinate system, the phase propagates to the right at speed $1/s_r$. For definiteness, we shall always take ω_r and ω_i to be non-negative; s_r and s_i are non-negative by definition. Representative plots are obtained with $(s_r, s_i, s_0) = (\sqrt{2}, 1, 1)$, $(\omega_r, \omega_i, \omega_0) = (1, 1, \sqrt{2})$, $p_0 = 1$, $t = 0$. In figure 1(*a*), the contours $p_r = 0$ are the upward-sloping straight lines $\theta_r = (n + \frac{1}{2})\pi$, with n integral, and have slope $\omega_r s_r/(\omega_i s_i)$. The contours with a given non-zero value of $|p_r|$ all touch a downward-sloping straight line corresponding to a fixed value of θ_i; such a straight line, parallel to ABC in the figure, has slope $-\omega_i s_r/(\omega_r s_i)$. Thus as evident from (2.13), at a fixed time the pressure does not oscillate in the direction θ_r = constant, and does not grow

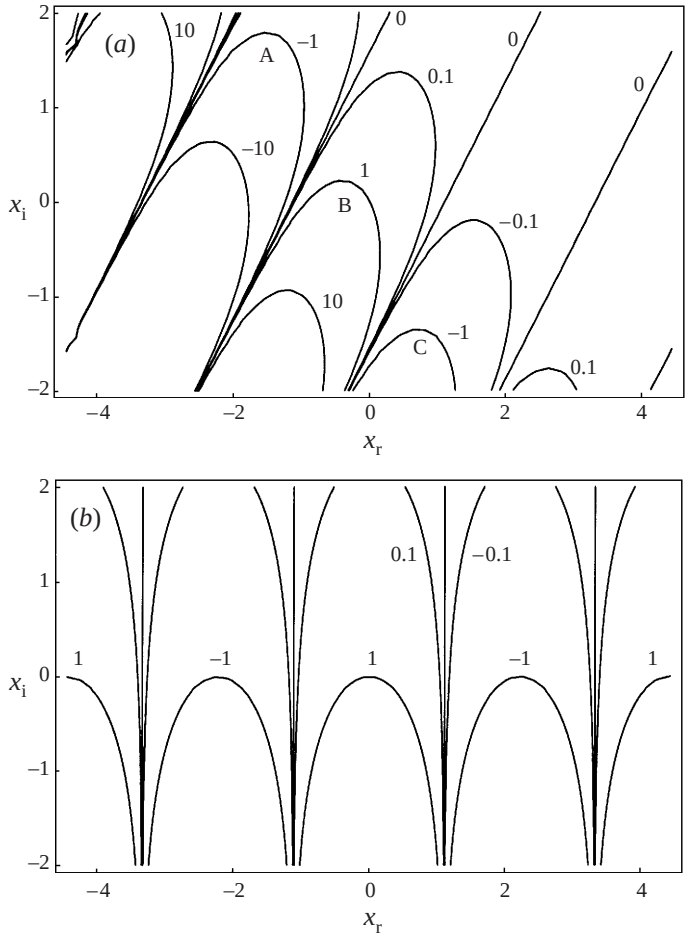

FIGURE 1. (*a*) Pressure contours $p_r = 0,\ \pm 0.1,\ \pm 1,\ \pm 10$ for $(\omega_r, \omega_i, \omega_0) = (1, 1, \sqrt{2})$, $(s_r, s_i, s_0) = (\sqrt{2}, 1, 1)$, $p_0 = 1$, $t = 0$. Thus $\theta_r = \sqrt{2}x_r - x_i$, $\theta_i = \sqrt{2}x_r + x_i$, $p_r = e^{-\theta_i}\cos\theta_r$, and the pattern propagates to the right at speed $1/s_r = 1/\sqrt{2}$. Contours with a given non-zero value of $|p_r|$ touch a straight line, parallel to ABC, of slope $-\omega_i s_r/(\omega_r s_i) = -\sqrt{2}$. The contours $p_r = 0$ are straight lines with slope $\omega_r s_r/(\omega_i s_i) = \sqrt{2}$. (*b*) As (*a*), but for a steady wave with $(\omega_r, \omega_i, \omega_0) = (1, 0, 1)$; contours are $p_r = 0,\ \pm 0.1,\ \pm 1$. Thus $(k_r, k_i) = (\sqrt{2}, 1)$, $\theta_r = \sqrt{2}x_r$, and $\theta_i = x_i$. The contours $p_r = 0$ are vertical straight lines.

or decay in the direction $\theta_i = \text{constant}$. The directions of $\boldsymbol{k}_r$ and $\boldsymbol{k}_i$ are given by (2.10). For example, if ω_r and ω_i are positive, then $\boldsymbol{k}_r$ points to the right and downwards, while $\boldsymbol{k}_i$ points to the right and upwards.

In the (x_r, x_i)-plane in figure 1(*a*), an edge wave may be specified by selecting a half-plane with a straight-line edge. This edge need not be parallel to the x_r-axis. The position and direction of the edge determine the variation of θ_r and θ_i along the edge. Thus in a particular problem, the boundary conditions determine where in figure 1(*a*) the edge should be taken, and how long a segment of the edge is relevant to the problem. A radiation condition determines on which side of the edge the half-plane should be taken. For example, if a region has an oscillating unstable boundary, the position of the edge in figure 1(*a*) is determined by the spatial and temporal growth rates of the instability. That is, with suitable values of $\omega_r, \omega_i, \boldsymbol{k}_r$, and $\boldsymbol{k}_i$, subject to the dispersion relation (2.4), the edge may be so placed to match the boundary conditions.

Thus the angle between the boundary and the straight-line contours $p_r = 0$ depends on the strength of the instability. If the unstable boundary is that of a jet issuing from a nozzle, the relevant part of the boundary is a finite segment from the end of the nozzle to the region where nonlinear effects can no longer be ignored. Such a segment, and the adjacent edge wave, are visible in photographs (e.g. Tam 1971, figure 7).

2.2. *Energy velocity; the hodograph*

In a fluid with undisturbed density ρ_0, the momentum equation shows that the acoustic velocity in the wave (2.1) is $\boldsymbol{u} = \rho_0^{-1}(\boldsymbol{k}/\omega)p$. Let us put $p_0 = \epsilon\rho_0 c_0^2$, where $\epsilon \ll 1$. Then in terms of the slowness $\boldsymbol{s} = \boldsymbol{k}/\omega$, we have

$$\boldsymbol{u} = \epsilon c_0^2 \boldsymbol{s} e^{i(\boldsymbol{k}\cdot\boldsymbol{x}-\omega t)} = \epsilon c_0^2(\boldsymbol{s}_r + i\boldsymbol{s}_i)e^{-\theta_i + i\theta_r}. \tag{2.15}$$

Therefore the real part $\boldsymbol{u}_r$ of $\boldsymbol{u}$ is

$$\boldsymbol{u}_r = \epsilon c_0^2 e^{-\theta_i}(\boldsymbol{s}_r \cos\theta_r - \boldsymbol{s}_i \sin\theta_r). \tag{2.16}$$

The energy flux transmitted by the wave, i.e. the energy transmitted per unit area per unit time, is the intensity $\boldsymbol{I} = p_r \boldsymbol{u}_r$. Equations (2.13) and (2.16) give

$$\begin{aligned}\boldsymbol{I} &= \epsilon p_0 c_0^2 e^{-2\theta_i}(\cos\theta_r)(\boldsymbol{s}_r\cos\theta_r - \boldsymbol{s}_i\sin\theta_r)\\ &= \tfrac{1}{2}\epsilon p_0 c_0^2 e^{-2\theta_i}\{\boldsymbol{s}_r(1+\cos 2\theta_r) - \boldsymbol{s}_i \sin 2\theta_r\}.\end{aligned} \tag{2.17}$$

The divergence $\nabla\cdot\boldsymbol{I}$ of the intensity is

$$\nabla\cdot\boldsymbol{I} = -\epsilon p_0 e^{-2\theta_i}\left\{\omega_r \sin 2\theta_r + \omega_i\left(\frac{s_r^2}{s_0^2} + \cos 2\theta_r\right)\right\}. \tag{2.18}$$

The kinetic and potential energy of the wave, per unit volume, are $\frac{1}{2}\rho_0 \boldsymbol{u}_r\cdot\boldsymbol{u}_r$ and $\frac{1}{2}(\rho_0 c_0^2)^{-1}p_r^2$. Their total W is

$$W = \tfrac{1}{2}\epsilon p_0 c_0^2 e^{-2\theta_i}(s_r^2 + s_0^2\cos 2\theta_r). \tag{2.19}$$

Calculation of $\partial W/\partial t$, and comparison with (2.18), confirm that $\boldsymbol{I}$ and W satisfy the equation of conservation of acoustic energy, namely

$$\frac{\partial W}{\partial t} + \nabla\cdot\boldsymbol{I} = 0. \tag{2.20}$$

The energy velocity is

$$\boldsymbol{U} = \frac{\boldsymbol{I}}{W} = \frac{2(\cos\theta_r)(\boldsymbol{s}_r\cos\theta_r - \boldsymbol{s}_i\sin\theta_r)}{s_r^2 + s_0^2\cos 2\theta_r}. \tag{2.21}$$

Therefore the energy paths are the solutions $(x_r(t), x_i(t))$ of

$$\dot{x}_r = \frac{s_r(1+\cos 2\theta_r)}{s_r^2 + s_0^2\cos 2\theta_r}, \qquad \dot{x}_i = \frac{-s_i \sin 2\theta_r}{s_r^2 + s_0^2\cos 2\theta_r}, \tag{2.22}$$

where, by (2.14), $\theta_r = \omega_r s_r x_r - \omega_i s_i x_i - \omega_r t$. We solve these equations in § 2.4.1.

With $\boldsymbol{U} = (U_r, U_i)$, (2.21) gives

$$\frac{U_i}{U_r} = -\frac{s_i}{s_r}\tan\theta_r, \qquad (s_r^2 + s_0^2)U_r^2 - 2s_r U_r + s_r^2 U_i^2 = 0. \tag{2.23a, b}$$

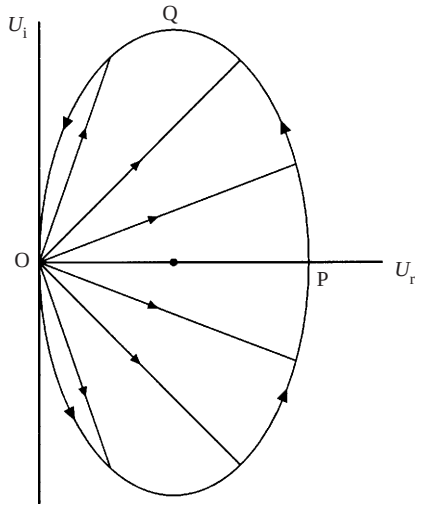

FIGURE 2. The tip of the energy velocity arrow from $(0,0)$ to (U_r, U_i) moves anti-clockwise around the ellipse (2.23*b*) in the hodograph plane, taking a time π/ω_r for one complete revolution. The rightmost point P of the ellipse is at $(2s_r/(s_r^2+s_0^2),0)$ and the highest point Q is at $(s_r/(s_r^2+s_0^2), 1/(s_r^2+s_0^2)^{1/2})$.

Also from (2.21), we obtain

$$\frac{|\boldsymbol{U}|^2}{c_0^2} = 1 - \left(\frac{s_i^2}{s_r^2 + s_0^2\cos 2\theta_r}\right)^2. \tag{2.24}$$

Equation (2.23*b*) defines an ellipse in the (U_r, U_i)-plane, i.e. in the energy hodograph plane. This ellipse, which passes through the origin and is centred at $(s_r/(s_r^2+s_0^2), 0)$, has height $2/(s_r^2+s_0^2)^{1/2}$ and width $2s_r/(s_r^2+s_0^2)$. Therefore the ratio of its height to width is $(s_r^2+s_0^2)^{1/2}/s_r$. Since this exceeds 1, the ellipse is taller that it is wide, i.e. its major axis is vertical and its minor axis is horizontal. An arrow from the origin to a point on the ellipse represents energy velocity. At a fixed position (x_r, x_i), equation (2.12*a*) shows that θ_r varies as $-\omega_r t$, so that, by (2.23*a*), the tip of the arrow moves anti-clockwise round the ellipse, as illustrated in figure 2. The period for one revolution is π/ω_r. Equation (2.24) shows that $|\boldsymbol{U}| \leqslant c_0$, i.e. that the energy velocity never exceeds the speed of sound c_0.

2.3. *Energy streamlines*

The energy streamlines at time $t_1 = 0$ are obtained by solving (2.22) with $\theta_r = \omega_r s_r x_r - \omega_i s_i x_i$. The ratio of the equations in (2.22) is

$$\frac{\mathrm{d}x_i}{\mathrm{d}x_r} = -\frac{s_i}{s_r}\tan(\omega_r s_r x_r - \omega_i s_i x_i). \tag{2.25}$$

Therefore the streamline pattern repeats itself at intervals of $\pi/(\omega_r s_r)$ in the x_r-direction, and contains straight-line streamlines of slope $\omega_r s_r/(\omega_i s_i)$ intercepting the x_r-axis at the points $(\omega_r s_r)^{-1}(n\pi - \tan^{-1}\{\omega_r s_r^2/(\omega_i s_i^2)\})$, $n = 0, \pm 1, \ldots$. (We shall omit the word 'energy' from terms such as energy streamline or energy streak line where the meaning is clear.) Wherever $\cos\theta_r = 0$, the velocity field has a singular point, i.e. $\mathrm{d}\boldsymbol{x}/\mathrm{d}t = 0$. Thus the singular points occupy the family of curves $\theta_r = (n+\frac{1}{2})\pi$, $n = 0, \pm 1, \ldots$, i.e. straight lines of slope $\omega_r s_r/(\omega_i s_i)$ intercepting the x_r-axis at the points $(n+\frac{1}{2})\pi/(\omega_r s_r)$. Phase-plane analysis shows that the streamlines approach the

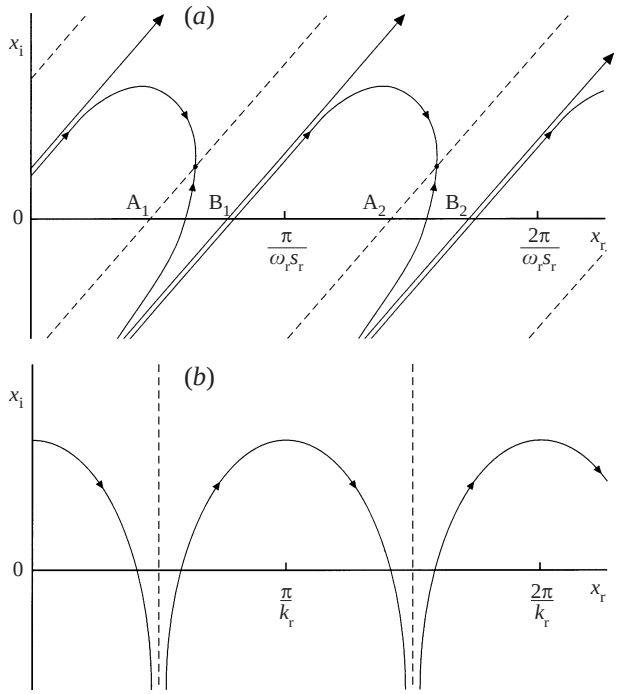

FIGURE 3. (*a*) Typical energy streamlines (——) at time $t_1 = 0$, including straight-line energy streamlines intersecting the x_r-axis at $B_1 : x_r = \{\pi - \tan^{-1}(\omega_r s_r^2/(\omega_i s_i^2))\}/(\omega_r s_r)$ and at B_2 a distance $\pi/(\omega_r s_r)$ to the right of B_1. The lines of singular points (----), where the energy velocity is instantaneously zero, intersect the x_r-axis at $A_1 : x_r = \frac{1}{2}\pi/(\omega_r s_r)$ and at $A_2 : x_r = \frac{3}{2}\pi/(\omega_r s_r)$. The straight lines in the figure have slope $\omega_r s_r/(\omega_i s_i)$. (*b*) As (*a*) but for a steady edge wave, i.e. $\omega_i = 0$ and $\omega_r s_r = k_r$. The straight-line energy streamlines have become lines of singular points (----) by merging with the original lines of singular points. Thus B_1 has become coincident with A_1 at $x_r = \frac{1}{2}\pi/k_r$; likewise B_2 with A_2 at $\frac{3}{2}\pi/k_r$.

singular points vertically. The streamlines are horizontal where they meet straight lines of slope $\omega_r s_r/(\omega_i s_i)$ intersecting the x_r-axis at the points $n\pi/(\omega_r s_r)$, $n = 0, \pm 1, \ldots$ Typical energy streamlines, including the direction of energy flow, are shown for $t_1 = 0$ in figure 3(*a*). The complete streamline pattern for $t_1 = 0$ is obtained by giving these streamlines every possible translation in the direction of the sloping straight lines in the figure. Most of the streamlines form parts of inverted slanted 'U' shapes, on which the energy flow is towards the singular point on each U. The exceptions are the straight-line streamlines, on which the energy flow is always upwards and to the right. Since the streamline pattern translates to the right at speed $1/s_r$, the figure determines the streamline pattern at all times.

2.4. *Energy paths*

2.4.1. *The equation of the energy paths*

The energy paths are obtained by solving (2.22). The time derivative of θ_r is

$$\dot{\theta}_r = \omega_r s_r \dot{x}_r - \omega_i s_i \dot{x}_i - \omega_r \tag{2.26}$$

$$= \frac{s_i^2(\omega_r \cos 2\theta_r + \omega_i \sin 2\theta_r)}{s_r^2 + s_0^2 \cos 2\theta_r}. \tag{2.27}$$

It is convenient to define 'up-angles' θ_u by the identity

$$\omega_r \cos 2\theta_r + \omega_i \sin 2\theta_r \equiv \omega_0 \sin 2(\theta_r - \theta_u). \tag{2.28}$$

This requires $\omega_r = -\omega_0 \sin 2\theta_u$ and $\omega_i = \omega_0 \cos 2\theta_u$, so that the up-angles are

$$\theta_u = n\pi - \tfrac{1}{2}\tan^{-1}\left(\frac{\omega_r}{\omega_i}\right), \qquad n = 0, \pm 1, \dots . \tag{2.29}$$

The reason for the name up-angle is that corresponding to the values $\theta_r = \theta_u$ are straight-line energy paths on which the vertical component of energy flow is upwards; see the remarks after (2.33) and (2.34). Division of $(\dot{x}_r, \dot{x}_i)$ by $\dot{\theta}_r$ gives the equations for the energy paths parametrically in terms of θ_r as

$$\frac{dx_r}{d\theta_r} = \frac{s_r(1 + \cos 2\theta_r)}{\omega_0 s_i^2 \sin 2(\theta_r - \theta_u)}, \qquad \frac{dx_i}{d\theta_r} = \frac{-\sin 2\theta_r}{\omega_0 s_i \sin 2(\theta_r - \theta_u)}, \tag{2.30a, b}$$

$$\frac{dt}{d\theta_r} = \frac{s_r^2 + s_0^2 \cos 2\theta_r}{\omega_0 s_i^2 \sin 2(\theta_r - \theta_u)}. \tag{2.30c}$$

Integration of these equations shows that the energy path which passes through the point (x_{r0}, x_{i0}) at time t_0 is

$$\frac{\omega_0 s_i^2}{s_r}(x_r - x_{r0}) = \frac{\omega_r}{\omega_0}(\theta_r - \theta_{r0}) + \frac{\omega_i}{2\omega_0} \ln\left|\frac{\sin 2(\theta_r - \theta_u)}{\sin 2(\theta_{r0} - \theta_u)}\right| + \frac{1}{2}\ln\left|\frac{\tan(\theta_r - \theta_u)}{\tan(\theta_{r0} - \theta_u)}\right|, \tag{2.31a}$$

$$\omega_0 s_i (x_i - x_{i0}) = -\frac{\omega_i}{\omega_0}(\theta_r - \theta_{r0}) + \frac{\omega_r}{2\omega_0} \ln\left|\frac{\sin 2(\theta_r - \theta_u)}{\sin 2(\theta_{r0} - \theta_u)}\right|, \tag{2.31b}$$

$$\frac{\omega_0 s_i^2}{s_0^2}(t - t_0) = \frac{\omega_r}{\omega_0}(\theta_r - \theta_{r0}) + \frac{\omega_i}{2\omega_0} \ln\left|\frac{\sin 2(\theta_r - \theta_u)}{\sin 2(\theta_{r0} - \theta_u)}\right| + \frac{s_r^2}{2s_0^2} \ln\left|\frac{\tan(\theta_r - \theta_u)}{\tan(\theta_{r0} - \theta_u)}\right|. \tag{2.31c}$$

Here the parameter θ_r, an 'unwrapped' phase angle, may range over $(-\infty, \infty)$, to cover all times, and the constant θ_{r0} is defined by

$$\theta_{r0} = \omega_r s_r x_{r0} - \omega_i s_i x_{i0} - \omega_r t_0. \tag{2.32}$$

A check of the calculation is that x_r, x_i, t, given by (2.31), satisfy identically the relation $\theta_r = \omega_r s_r x_r - \omega_i s_i x_i - \omega_r t$. In principle, elimination of θ_r from (2.31) gives the energy path in the form $(x_r(t), x_i(t))$; but such elimination is not possible analytically.

2.4.2. *Straight-line energy paths*

Equations (2.30*a, b*) or (2.22) give

$$\frac{dx_i}{dx_r} = -\frac{s_i}{s_r}\tan\theta_r. \tag{2.33}$$

Therefore the energy paths are straight lines if $\dot{\theta}_r = 0$ for all t, i.e. if $\sin 2(\theta_r - \theta_u) = 0$. This requires $\theta_r = \theta_u + \frac{1}{2}m\pi$, $m = 0, \pm 1, \dots$. First let m be even, so that

$$\dot{x}_r = \frac{(\omega_0 + \omega_i)s_r}{\omega_0 s_r^2 + \omega_i s_0^2}, \qquad \dot{x}_i = \frac{\omega_r s_i}{\omega_0 s_r^2 + \omega_i s_0^2}, \qquad \frac{dx_i}{dx_r} = \left(\frac{\omega_r}{\omega_0 + \omega_i}\right)\frac{s_i}{s_r}. \tag{2.34a–c}$$

Then $\dot{x}_r, \dot{x}_i$ and dx_i/dx_r are all positive, and the energy flow is upwards along the straight line. (The term 'upwards' will always mean 'with an upwards component' not 'vertically upwards'.) The expression $\theta_r = \theta_u + \frac{1}{2}m\pi$ may be written when m is even as $\theta_r = n'\pi - \frac{1}{2}\tan^{-1}(\omega_r/\omega_i)$, $n' = 0, \pm 1, \ldots$, and then gives the same set of values as (2.29); hence the term up-angles for the values of θ_u. Now let m be odd. Then

$$\dot{x}_r = \frac{(\omega_0 - \omega_i)s_r}{\omega_0 s_r^2 - \omega_i s_0^2}, \qquad \dot{x}_i = \frac{-\omega_r s_i}{\omega_0 s_r^2 - \omega_i s_0^2}, \qquad \frac{dx_i}{dx_r} = -\left(\frac{\omega_r}{\omega_0 - \omega_i}\right)\frac{s_i}{s_r}. \quad (2.35a\text{–}c)$$

Thus $\dot{x}_r$ is still positive, but $\dot{x}_i$ and dx_i/dx_r are negative, i.e. the energy flow is downwards along the straight line. The expression for θ_r with m odd may be written $\theta_r = (n' + \frac{1}{2})\pi - \frac{1}{2}\tan^{-1}(\omega_r/\omega_i)$, $n' = 0, \pm 1, \ldots$. These values may be called down-angles θ_d, so that, apart from multiples of π,

$$\theta_d = \theta_u + \tfrac{1}{2}\pi. \quad (2.36)$$

The downwards straight-line energy paths are at a steeper angle to the horizontal direction than are the upwards straight-line paths. This follows from comparing the denominators in (2.34*c*) and (2.35*c*). Since $s_r > s_i$, and we are assuming $\omega_r > 0$, the angle between the upwards path and the horizontal is less than 45°. It may be checked that the energy velocities $\boldsymbol{U} = (U_r, U_i) = (\dot{x}_r, \dot{x}_i)$ obtained from (2.34) and (2.35) satisfy the hodograph relations (2.23)–(2.24).

2.4.3. *Limiting directions of energy paths*

The straight-line energy paths determine the limiting directions, as $t \to \pm\infty$, of an arbitrary energy path. The limit $\theta_r \to \theta_u$ in (2.31) gives (except when $\theta_{r0} = \theta_u$ or θ_d)

$$\frac{\omega_0 s_i^2 x_r}{s_r} \approx \left(\frac{\omega_0 + \omega_i}{2\omega_0}\right)\ln|\theta_r - \theta_u| \to -\infty, \quad \omega_0 s_i x_i \approx \frac{\omega_r}{2\omega_0}\ln|\theta_r - \theta_u| \to -\infty, \quad (2.37a, b)$$

$$\frac{\omega_0 s_i^2 t}{s_0^2} \approx \frac{1}{2}\left(\frac{s_r^2}{s_0^2} + \frac{\omega_i}{\omega_0}\right)\ln|\theta_r - \theta_u| \to -\infty, \quad (2.37c)$$

i.e.

$$\frac{x_i}{x_r} \to \left(\frac{\omega_r}{\omega_0 + \omega_i}\right)\frac{s_i}{s_r}, \qquad t \to -\infty. \quad (2.38)$$

Similarly, the limit $\theta_r \to \theta_d$ gives (except when $\theta_{r0} = \theta_u$ or θ_d)

$$\frac{\omega_0 s_i^2 x_r}{s_r} \approx -\left(\frac{\omega_0 - \omega_i}{2\omega_0}\right)\ln|\theta_r - \theta_d| \to \infty, \quad \omega_0 s_i x_i \approx \frac{\omega_r}{2\omega_0}\ln|\theta_r - \theta_d| \to -\infty, \quad (2.39a, b)$$

$$\frac{\omega_0 s_i^2 t}{s_0^2} \approx -\frac{1}{2}\left(\frac{s_r^2}{s_0^2} - \frac{\omega_i}{\omega_0}\right)\ln|\theta_r - \theta_d| \to \infty, \quad (2.39c)$$

i.e.

$$\frac{x_i}{x_r} \to -\left(\frac{\omega_r}{\omega_0 - \omega_i}\right)\frac{s_i}{s_r}, \qquad t \to \infty. \quad (2.40)$$

The exceptional cases $\theta_{r0} = \theta_u$ or θ_d correspond to an upwards or downwards straight-line energy path. Thus at large negative times, all energy paths except the discrete set of downwards straight-line paths are asymptotically parallel to the upwards straight-line paths. At large positive times, all energy paths except the discrete set of upwards straight-line paths are asymptotically parallel to the downwards straight-line paths. The limiting energy velocity is that of the energy on these straight-line paths. Since the amount of energy carried along a single path in a continuum of paths is zero, we may say that, if energy paths are extended to the range $-\infty < t < \infty$, then all of the energy originates in the lower left region, moving upwards and right, and ends in the lower right region, moving downwards and right.

2.4.4. *Cusps on energy paths*

An energy path has a cusp where $\dot{x}_r = \dot{x}_i = 0$, i.e. $\cos\theta_r = 0$. This occurs at $\theta_r = \theta_{rc} \equiv (n + \frac{1}{2})\pi$, $n = 0, \pm 1, \ldots$, where (2.30) gives

$$\frac{dx_r}{d\theta_r} = 0, \quad \frac{d^2x_r}{d\theta_r^2} = 0, \quad \frac{d^3x_r}{d\theta_r^3} = -\frac{4s_r}{\omega_r s_i^2}, \quad \frac{dx_i}{d\theta_r} = 0, \quad \frac{d^2x_i}{d\theta_r^2} = -\frac{2}{\omega_r s_i}, \quad \frac{dt}{d\theta_r} = -\frac{1}{\omega_r}. \tag{2.41}$$

The values of (x_r, x_i, t) at a cusp will be denoted (x_{rc}, x_{ic}, t_c) and are obtained from (2.31) by putting $\theta_r = \theta_{rc}$. The energy path near a cusp is

$$x_r - x_{rc} \approx -\frac{2s_r}{3\omega_r s_i^2}(\theta_r - \theta_{rc})^3, \quad x_i - x_{ic} \approx -\frac{1}{\omega_r s_i}(\theta_r - \theta_{rc})^2, \quad t - t_c \approx -\frac{1}{\omega_r}(\theta_r - \theta_{rc}), \tag{2.42}$$

or equivalently

$$x_r - x_{rc} \approx \frac{2\omega_r^2 s_r}{3s_i^2}(t - t_c)^3, \qquad x_i - x_{ic} \approx -\frac{\omega_r}{s_i}(t - t_c)^2. \tag{2.43}$$

Thus

$$(x_i - x_{ic})^3 \approx -\frac{9s_i}{4\omega_r s_r^2}(x_r - x_{rc})^2. \tag{2.44}$$

The cusps all point vertically upwards, and the energy path is below the horizontal line $x_i = x_{ic}$.

2.4.5. *Energy paths from a point; domains of influence and dependence*

We now describe all the energy paths from the point $(x_{r0}, x_{i0}) = (0, 0)$. Thus $\theta_{r0} = -\omega_r t_0$, where t_0 is the starting time. From the periodicity of the differential equations (2.30), the paths are generated by an interval $-\pi \leqslant \theta_{r0} \leqslant 0$, i.e. $0 \leqslant t_0 \leqslant \pi/\omega_r$. The initial energy velocity at $(0, 0)$ varies with t_0 as in the hodograph diagram shown in figure 2. A set of paths is shown in figure 4(*a*) for $t_0 \leqslant t \leqslant \frac{5}{2}\pi/\omega_r$, each path corresponding to a different starting time t_0 in the interval $0 \leqslant t_0 \leqslant \pi/\omega_r$. Although we have taken $(x_{r0}, x_{i0}) = (0, 0)$, the results are identical for all values of (x_{r0}, x_{i0}), except for a phase difference.

The energy paths are given by (2.31). The union of all the paths for $0 \leqslant t_0 \leqslant \pi/\omega_r$ and $t \geqslant t_0$ fills the region which can be reached by energy from $(0, 0)$. This region is the domain of influence of $(0, 0)$. It is the region which would be covered by the energy paths in figure 4(*a*) if each path were extended to infinity (by taking $t \to \infty$) and an infinite number of paths were included (one for every t_0 in the interval $0 \leqslant t_0 \leqslant \pi/\omega_r$).

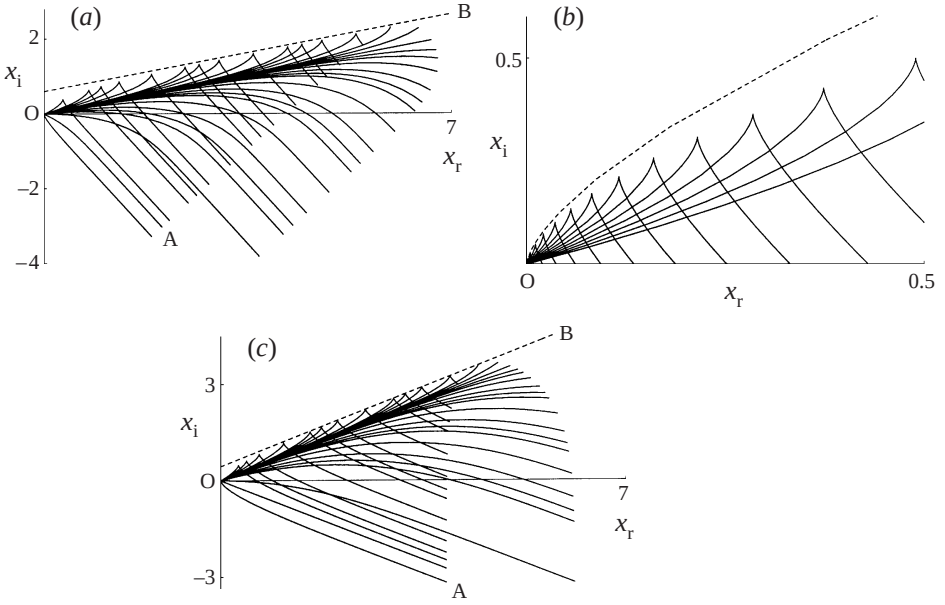

FIGURE 4. (a) Energy paths from $(0,0)$ for $(\omega_r, \omega_i, \omega_0) = (1, 1, \sqrt{2})$, $(s_r, s_i, s_0) = (\sqrt{2}, 1, 1)$. Starting times t_0 lie in the range $0 \leqslant t_0 \leqslant \pi/\omega_r$, and each path is drawn for $t_0 \leqslant t \leqslant \frac{5}{2}\pi/\omega_r$. The path OA leaves $(0,0)$ vertically downwards, and the dashed line is the asymptote (2.46) of the locus of cusps. (*b*) Further detail near $(0,0)$. The dashed line is $x_i^3 = (9s_i/(4\omega_r s_r^2))x_r^2$, an approximation to the locus of cusps near $(0,0)$. (*c*) As (*a*), but for a steady wave with $(\omega_r, \omega_i, \omega_0) = (1, 0, 1)$.

Thus the domain of influence is an infinitely long wedge with curved boundaries; these are the extensions to infinity of the curves marked OA and OB. Similarly, the union of all the energy paths before they reach $(0,0)$ fills the region from which energy can originate if it is to pass through $(0,0)$. This region is the domain of dependence of $(0,0)$. It is not shown in figure 4(*a*), but would be similar to the mirror image, in the x_i-axis, of the domain of influence.

The lower boundary of the domain of influence of $(0,0)$, i.e. OA and its extension, is the energy path which leaves $(0,0)$ vertically downwards. This boundary is the right half of a path with a cusp at $(0,0)$, and is the path for which $t_0 = \frac{1}{2}\pi/\omega_r$. Hence its equation is (2.31) with $(x_{r0}, x_{i0}, t_0) = (0, 0, \frac{1}{2}\pi/\omega_r)$ and $\theta_{r0} = -\frac{1}{2}\pi$. Its asymptote far from the origin is

$$x_i + \left(\frac{\omega_r}{\omega_0 - \omega_i}\right)\frac{s_i}{s_r}x_r = \frac{\theta_u}{\omega_0 s_i} + \frac{1}{2}\left(\frac{\omega_r}{\omega_0 - \omega_i}\right)\frac{1}{\omega_0 s_i}\ln\left(\frac{2\omega_0}{\omega_0 + \omega_i}\right). \tag{2.45}$$

Hence the asymptote intersects the x_i-axis at the value of x_i given by the right-hand side of (2.45), which for the parameter values in figure 4(*a*) is $x_i = -0.14252$. The asymptote is indistinguishable from the actual path except very close to the origin, where the path is curved. An approximation to this curved path is $x_i^3 = -(9s_i/(4\omega_r s_r^2))x_r^2$.

The upper boundary of the domain of influence in figure 4(*a*) is the line of cusps. These occur where $\theta_r = -\frac{1}{2}\pi$ and lie on energy paths with $-\theta_u/\omega_r \leqslant t_0 \leqslant \frac{1}{2}\pi/\omega_r$. Therefore the equation of the line of cusps is (2.31) with $(x_{r0}, x_{i0}, \theta_r) = (0, 0, -\frac{1}{2}\pi)$ and θ_{r0} taken to vary from $-\frac{1}{2}\pi$ to $-\frac{1}{2}\tan^{-1}(\omega_r/\omega_i)$; in (2.31) it is necessary to put

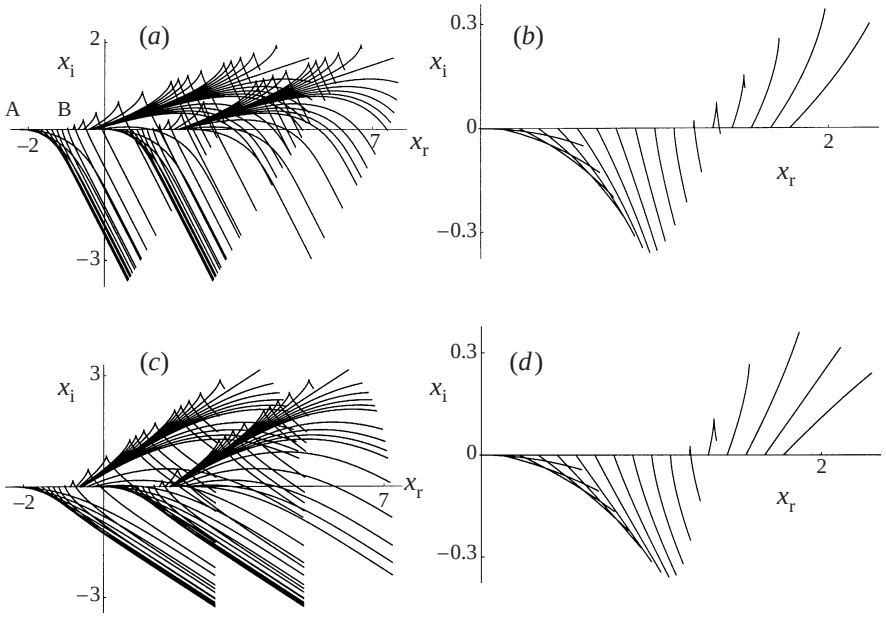

FIGURE 5. Energy paths from the segment $|x_r| \leqslant \pi/(\omega_r s_r)$ of the x_r-axis at time $t_0 = 0$, for $(\omega_r, \omega_i, \omega_0) = (1, 1, \sqrt{2})$, $(s_r, s_i, s_0) = (\sqrt{2}, 1, 1)$. (*a*) Paths from many values of x_r, drawn for $0 \leqslant t \leqslant 2\pi/\omega_r$. (*b*) Further detail near the positive x_r-axis for $0 \leqslant t \leqslant \frac{1}{5}\pi/\omega_r$. (*c*, *d*) As (*a*, *b*), but for a steady wave with $(\omega_r, \omega_i, \omega_0) = (1, 0, 1)$.

$t_0 = -\theta_{r0}/\omega_r$. The asymptote far from the origin is

$$x_i - \left(\frac{\omega_r}{\omega_0 + \omega_i}\right)\frac{s_i}{s_r}x_r = \frac{\frac{1}{2}\pi + \theta_u}{\omega_0 s_i} - \frac{1}{2}\left(\frac{\omega_r}{\omega_0 + \omega_i}\right)\frac{1}{\omega_0 s_i}\ln\left(\frac{2\omega_0}{\omega_0 - \omega_i}\right). \tag{2.46}$$

Hence the asymptote intersects the x_i-axis at the value of x_i given by the right-hand side of (2.46), which for the parameter values in figure 4(*a*) is $x_i = 0.55170$. The asymptote is shown as the upper dashed line in the figure; the distance from the asymptote to the cusps is appreciable only very close to the origin. Near the origin, an approximation to the position of the cusps is $x_i^3 = (9s_i/(4\omega_r s_r^2))x_r^2$, as shown in figure 4(*b*).

2.4.6. *Energy paths from a segment*

Energy paths leaving the segment $|x_r| \leqslant \pi/(\omega_r s_r)$ of the x_r-axis at time $t_0 = 0$ are shown in figure 5(*a*). As the spatial period in the x_r-direction is $\pi/(\omega_r s_r)$, paths leaving $0 \leqslant x_r \leqslant \pi/(\omega_r s_r)$ are the same size and shape as those leaving $-\pi/(\omega_r s_r) \leqslant x_r \leqslant 0$. Energy leaves downwards from $-\pi/(\omega_r s_r) < x_r < -\frac{1}{2}\pi/(\omega_r s_r)$ and from $0 < x_r < \frac{1}{2}\pi/(\omega_r s_r)$. This is especially evident at the horizontal boundary AB towards the left of figure 5(*a*) and in the detail, shown in figure 5(*b*), of a region near the positive x_r-axis. All energy paths ultimately head downwards, except for the discrete set of upwards straight-line paths.

2.4.7. *Moving coordinates*

The equations in this section may be expressed in moving coordinates (θ_r, θ_i) instead of the fixed coordinates (x_r, x_i). For example, the time derivative of θ_i is

$$\dot{\theta}_i = \omega_i s_r \dot{x}_r + \omega_r s_i \dot{x}_i - \omega_i = \frac{\omega_0 s_i^2 \cos 2(\theta_r - \theta_u)}{s_r^2 + s_0^2 \cos 2\theta_r}. \tag{2.47}$$

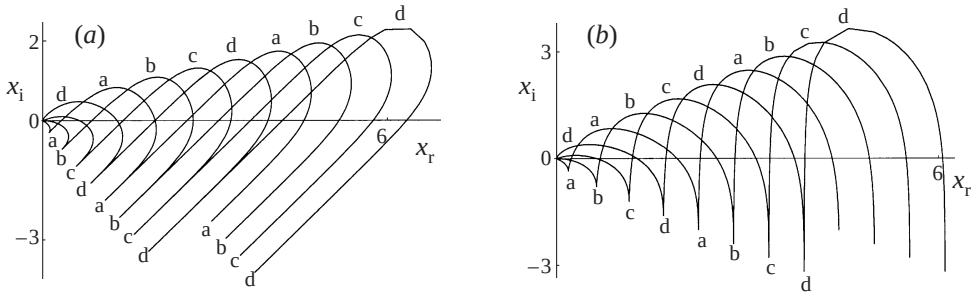

FIGURE 6. (*a*) Energy streak lines from (0, 0) for observation times $t_1 = \frac{1}{4}n\pi/\omega_r$, $n = 1, 2, \ldots, 10$ and departure times from 0 to t_1. The lines for $n = 7, 8, 9, 10$ are marked a, b, c, d; lines for $n = 1, 2, \ldots, 6$ are segments of c, d, a, b, c, d respectively. The frequency and slowness parameters are $(\omega_r, \omega_i, \omega_0) = (1, 1, \sqrt{2})$, $(s_r, s_i, s_0) = (\sqrt{2}, 1, 1)$. The extended and filled region of lines is the same as that of figure 4(*a*), i.e. is the domain of influence of (0, 0). (*b*) As (*a*), but for a steady wave with $(\omega_r, \omega_i, \omega_0) = (1, 0, 1)$.

Division by $\dot{\theta}_r$ gives

$$\frac{d\theta_i}{d\theta_r} = \cot 2(\theta_r - \theta_u). \tag{2.48}$$

Hence

$$\theta_i - \theta_{i0} = \frac{1}{2}\ln\left|\frac{\sin 2(\theta_r - \theta_u)}{\sin 2(\theta_{r0} - \theta_u)}\right|. \tag{2.49}$$

Here the constant θ_{i0} is defined by $\theta_{i0} = \omega_i s_r x_{r0} + \omega_r s_i x_{i0} - \omega_i t_0$. Equation (2.49) gives energy paths in a frame of reference moving with the pressure contours of p_r shown in figure 1, i.e. in a frame moving 'with the phase speed'. Thus (2.49) gives the 'drift' of energy relative to the phase lines. Equation (2.49) is also a simple consequence of (2.31) and the definition of θ_i. The (θ_r, θ_i)-coordinate system, though superficially attractive, is not orthogonal, and the main results in this section are most easily derived, as here, in the fixed orthogonal system (x_r, x_i) in which the ambient fluid is at rest.

2.5. *Energy streak lines*

At an observation time t_1, the energy particles which left a fixed point (x_{r0}, x_{i0}) at earlier times form a curve, the energy streak line at time t_1 from (x_{r0}, x_{i0}). A plot of such a streak line is obtained as follows: first (2.22) is solved with initial condition $(x_r(t_0), x_i(t_0)) = (x_{r0}, x_{i0})$, where t_0 is a parameter, namely the departure time; then $(x_r(t_1), x_i(t_1))$ is plotted for all t_0 with $t_0 \leqslant t_1$. Streak lines from (0, 0) are shown in figure 6(*a*) for various observation times t_1 in the range 0 to $\frac{5}{2}\pi/\omega_r$. Each streak line in the figure is for $0 \leqslant t_0 \leqslant t_1$ at fixed t_1. The streak lines consist of slanted U-shaped segments, joined at cusps. Each of these segments is larger than the one to the left, and extends further from the x_r-axis, both above and below it. For small t_1, only part of the first segment is present; as t_1 increases, the number of segments increases indefinitely.

The streak lines from (0, 0) for all t_1 fill a region consisting of all the points in space which can be reached by energy from (0, 0). This is simply the domain of influence of (0, 0), as defined in § 2.4.5, where it was constructed as the union of the energy paths from (0, 0). Thus a check of our calculations is that the extended and filled region of streak lines in figure 6(*a*) must be the same as the extended and filled region of path lines in figure 4(*a*), as the figures confirm. In § 2.4.5 we saw that the lower boundary

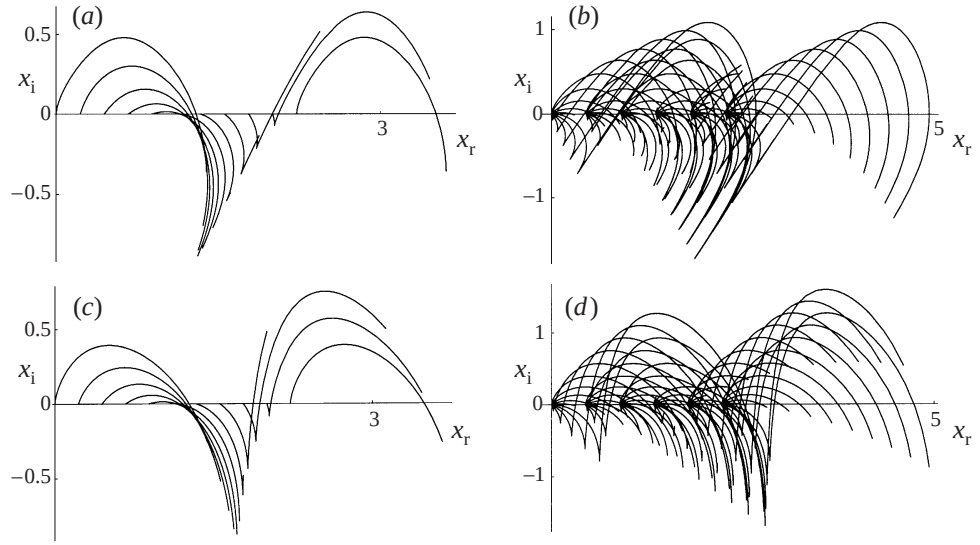

FIGURE 7. (*a*) Energy streak lines from points $x_r = 0, \frac{1}{10}\pi/(\omega_r s_r), \ldots, \pi/(\omega_r s_r)$ on the x_r-axis; observation time $\frac{1}{2}\pi/\omega_r$. (*b*) As (*a*), but with $x_r = 0, \frac{1}{5}\pi/(\omega_r s_r), \ldots, \pi/(\omega_r s_r)$ and observation times $\frac{1}{10}\pi/\omega_r, \frac{2}{10}\pi/\omega_r, \ldots, \pi/\omega_r$. Departure times are from 0 to the observation time. Frequency and slowness parameters: $(\omega_r, \omega_i, \omega_0) = (1, 1, \sqrt{2})$, $(s_r, s_i, s_0) = (\sqrt{2}, 1, 1)$. (*c*, *d*) As (*a*, *b*), but for a steady wave with $(\omega_r, \omega_i, \omega_0) = (1, 0, 1)$.

of the region is the energy path which leaves $(0, 0)$ vertically downwards; figure 6(*a*) shows that this boundary is equally the locus of cusps on streak lines. The upper boundary is the locus of cusps on energy paths, or equally an envelope of smooth parts of streak lines.

Energy streak lines from the segment $0 \leqslant x_r \leqslant \pi/(\omega_r s_r)$ of the x_r-axis are shown in figure 7(*a*) for the single observation time $\frac{1}{2}\pi/\omega_r$ and departure times from 0 to $\frac{1}{2}\pi/\omega_r$. Similarly constructed streak lines are superposed in figure 7(*b*) for observation times $\frac{1}{10}\pi/\omega_r, \frac{2}{10}\pi/\omega_r, \ldots, \pi/\omega_r$. The streak lines in figure 7(*a*) may be compared with the path lines in figure 5(*b*).

3. Steady edge waves

A wave is steady if the frequency ω is real, i.e. $\omega_i = 0$. Thus $\omega = \omega_r$ and the dispersion relation (2.2) for an edge wave becomes

$$\omega_r^2 = c_0^2(\boldsymbol{k}_r \cdot \boldsymbol{k}_r - \boldsymbol{k}_i \cdot \boldsymbol{k}_i), \qquad \boldsymbol{k}_r \cdot \boldsymbol{k}_i = 0. \tag{3.1a, b}$$

Hence $\boldsymbol{k}_r$ and $\boldsymbol{k}_i$ are perpendicular. (It may be checked that the edge wave given by equation (19) in Tam (1971) satisfies (3.1).) The definition (2.9) of ω_0 gives $\omega_0 = \omega_r = \omega$, so that, by (2.10*a*, *b*), the real and imaginary parts of the slowness vector are

$$\boldsymbol{s}_r = \boldsymbol{k}_r/\omega_0, \qquad \boldsymbol{s}_i = \boldsymbol{k}_i/\omega_0. \tag{3.2}$$

We put $k_r = |\boldsymbol{k}_r|$ and $k_i = |\boldsymbol{k}_i|$, so that $s_r = k_r/\omega_0$ and $s_i = k_i/\omega_0$. Then with k_0 defined by $k_0 = \omega_0 s_0 = \omega_0/c_0$, equation (3.1*a*) is

$$k_0^2 = k_r^2 - k_i^2. \tag{3.3}$$

The x_r-direction is that of $\boldsymbol{k}_r$, and the x_i-direction is that of $\boldsymbol{k}_i$, i.e. $\boldsymbol{k}_r = (k_r, 0)$ and $\boldsymbol{k}_i = (0, k_i)$. Equations (2.12) or (2.14) give

$$\theta_r = k_r x_r - \omega_0 t, \qquad \theta_i = k_i x_i. \tag{3.4}$$

The real part of the pressure is

$$p_r = p_0 e^{-\theta_i} \cos\theta_r = p_0 e^{-k_i x_i} \cos(k_r x_r - \omega_0 t). \tag{3.5}$$

Typical contours of p_r at a fixed time t are shown in figure 1(*b*). The phase propagates to the right at speed ω_0/k_r. Parameter values for plots of steady waves will be obtained from those for unsteady waves by taking $\omega_i = 0$ instead of $\omega_i = 1$. Thus in figure 1(*b*) we have $p_0 = 1$, $t = 0$, $(s_r, s_i, s_0) = (\sqrt{2}, 1, 1)$, and $(\omega_r, \omega_i, \omega_0) = (1, 0, 1)$, so that $(k_r, k_i) = (\sqrt{2}, 1)$ and $(\theta_r, \theta_i) = (\sqrt{2}x_r, x_i)$, whence $p_r = e^{-x_i}\cos(\sqrt{2}x_r)$. A steady edge wave corresponds in figure 1(*b*) to a half-plane with a straight-line edge; the edge need not be parallel to the x_r-axis. The relation between such a half-plane and the boundary conditions of a problem is as discussed at the end of § 2.1. The jet-noise photograph there referred to (Tam 1971, figure 7) is of a steady edge wave; the photograph shows not the energy paths themselves but the domain of influence of acoustic sources in the jet, and this domain has the shape and orientation predicted by our theory. A full analysis of the energy flow in this field would require a slight extension of the theory we are presenting, because the photograph shows a meridional section of a cylindrical sound field.

The energy paths are the solutions $(x_r(t), x_i(t))$ of

$$\dot{x}_r = \frac{\omega_0 k_r(1 + \cos 2\theta_r)}{k_r^2 + k_0^2 \cos 2\theta_r}, \qquad \dot{x}_i = \frac{-\omega_0 k_i \sin 2\theta_r}{k_r^2 + k_0^2 \cos 2\theta_r}, \tag{3.6}$$

and typical hodograph relations are

$$\frac{U_i}{U_r} = -\frac{k_i}{k_r}\tan\theta_r, \qquad (k_r^2 + k_0^2)U_r^2 - 2k_r k_0 c_0 U_r + k_r^2 U_i^2 = 0, \tag{3.7a,b}$$

$$\frac{|\boldsymbol{U}|^2}{c_0^2} = 1 - \left(\frac{k_i^2}{k_r^2 + k_0^2\cos 2\theta_r}\right)^2. \tag{3.7c}$$

Energy streamlines at time $t_1 = 0$ are shown in figure 3(*b*). The pattern has period π/k_r in the x_r-direction, and there are no longer any straight-line streamlines: as $\omega_i \to 0$ they become lines of singular points, with equations $x_r = (n - \frac{1}{2})\pi/k_r$, $n = 0, \pm 1, \ldots$, by merging with the original lines of singular points. The up-angles and down-angles are $\theta_u = (n - \frac{1}{4})\pi$ and $\theta_d = (n + \frac{1}{4})\pi$, $n = 0, \pm 1, \ldots$, and the energy paths are

$$\frac{k_i^2}{k_r}(x_r - x_{r0}) = \theta_r - \theta_{r0} + \frac{1}{2}\ln\left|\frac{\tan(\theta_r + \frac{1}{4}\pi)}{\tan(\theta_{r0} + \frac{1}{4}\pi)}\right|, \quad k_i(x_i - x_{i0}) = \frac{1}{2}\ln\left|\frac{\cos 2\theta_r}{\cos 2\theta_{r0}}\right|, \tag{3.8a,b}$$

$$\frac{\omega_0 k_i^2}{k_0^2}(t - t_0) = \theta_r - \theta_{r0} + \frac{1}{2}\frac{k_r^2}{k_0^2}\ln\left|\frac{\tan(\theta_r + \frac{1}{4}\pi)}{\tan(\theta_{r0} + \frac{1}{4}\pi)}\right|. \tag{3.8c}$$

On the upwards straight-line energy paths, (2.34) gives

$$\dot{x}_r = \frac{\omega_0}{k_r}, \qquad \dot{x}_i = \frac{\omega_0 k_i}{k_r^2}, \qquad \frac{\mathrm{d}x_i}{\mathrm{d}x_r} = \frac{k_i}{k_r}. \tag{3.9}$$

On the downwards straight-line paths, (2.35) gives

$$\dot{x}_\mathrm{r} = \frac{\omega_0}{k_\mathrm{r}}, \qquad \dot{x}_\mathrm{i} = -\frac{\omega_0 k_\mathrm{i}}{k_\mathrm{r}^2}, \qquad \frac{\mathrm{d}x_\mathrm{i}}{\mathrm{d}x_\mathrm{r}} = -\frac{k_\mathrm{i}}{k_\mathrm{r}}. \tag{3.10}$$

Thus the upwards and downwards straight-line paths are equally inclined to the horizontal direction. Since $k_\mathrm{i} < k_\mathrm{r}$, the angle to the horizontal direction is less than 45°. The energy speed $|\boldsymbol{U}|$ on a straight-line path, whether an upwards or a downwards path, satisfies $|\boldsymbol{U}|^2/c_0^2 = 1 - (k_\mathrm{i}/k_\mathrm{r})^4$. Every energy path, except a straight-line path, is symmetric about a vertical axis; on the left-hand side of this axis, the energy flows upwards, and on the right-hand side it flows downwards.

An energy path has a cusp where $\theta_\mathrm{r} = \theta_\mathrm{rc} = (n + \frac{1}{2})\pi$, $n = 0, \pm 1, \ldots$. At a cusp, the first non-zero derivatives of (3.8) are

$$\frac{\mathrm{d}^3 x_\mathrm{r}}{\mathrm{d}\theta_\mathrm{r}^3} = -\frac{4k_\mathrm{r}}{k_\mathrm{i}^2}, \qquad \frac{\mathrm{d}^2 x_\mathrm{i}}{\mathrm{d}\theta_\mathrm{r}^2} = -\frac{2}{k_\mathrm{i}}, \qquad \frac{\mathrm{d}t}{\mathrm{d}\theta_\mathrm{r}} = -\frac{1}{\omega_0}, \tag{3.11}$$

so that the energy path near a cusp $(x_\mathrm{rc}, x_\mathrm{ic})$ is

$$(x_\mathrm{i} - x_\mathrm{ic})^3 \approx -\frac{9k_\mathrm{i}}{4k_\mathrm{r}^2}(x_\mathrm{r} - x_\mathrm{rc})^2. \tag{3.12}$$

Energy paths from $(0,0)$ are shown in figure 4(c). The boundaries of the domain of influence of $(0,0)$ have asymptotes

$$x_\mathrm{i} \mp \frac{k_\mathrm{i}}{k_\mathrm{r}} x_\mathrm{r} = \pm\frac{1}{2k_\mathrm{i}}\left(\frac{\pi}{2} - \ln 2\right) \approx \pm\frac{0.4388}{k_\mathrm{i}}, \tag{3.13}$$

where the upper sign corresponds to the upper boundary. These asymptotes, of slopes $\pm k_\mathrm{i}/k_\mathrm{r}$, intersect the axes at $x_\mathrm{r} \approx -0.4388 k_\mathrm{r}/k_\mathrm{i}^2$ and $x_\mathrm{i} \approx \pm 0.4388/k_\mathrm{i}$. Since $k_\mathrm{i} < k_\mathrm{r}$, the angle between each asymptote and the horizontal axis is less than 45°, consistent with Jones (1977). Near the origin, the boundary is approximately $x_\mathrm{i}^3 = \pm(9k_\mathrm{i}/(4k_\mathrm{r}^2))x_\mathrm{r}^2$. Although these limiting forms are mirror-symmetric about the x_r-axis, the exact domain of influence has this symmetry only approximately. Energy paths leaving the segment $|x_\mathrm{r}| \leqslant \pi/k_\mathrm{r}$ of the x_r-axis at time $t_0 = 0$ are shown in figure 5(c,d). Equation (2.49), with $\theta_\mathrm{u} = -\frac{1}{4}\pi$, shows that a simple relation between θ_r and θ_i on an energy path is $\theta_\mathrm{i} - \theta_{\mathrm{i}0} = \frac{1}{2}\ln|\cos 2\theta_\mathrm{r}/\cos 2\theta_{\mathrm{r}0}|$. Energy streak lines from the point $(0,0)$ are shown in figure 6(b), and from the interval $0 \leqslant x_\mathrm{r} \leqslant \pi/k_\mathrm{r}$ of the x_r-axis in figure 7(c,d). The domain of influence of $(0,0)$ is the extended and filled region of streak lines in figure 6(b), or equivalently the extended and filled region of path lines in figure 4(c).

4. The physical significance of energy paths

Some readers might feel that only energy fluxes averaged over a wave period are important, and that instantaneous fluxes merely account for the periodic redistribution of energy within a given region. Thus the energy arrows in figure 2 point on average horizontally to the right, and one might think that the oscillation of the arrows could lead at most to an unimportant wiggle about the horizontal direction. The author believes this line of reasoning to be fallacious, because it ignores the long-range coherence of the phase of the wave field, both in space and time. When a succession of diagrams like figure 2 is used to construct an energy path by stepping forward in time, the direction of the arrow on the path, as a function of time, is found to be very different from the corresponding function of time at a fixed point, and does not even remotely resemble a periodic oscillation about a fixed direction. Nevertheless,

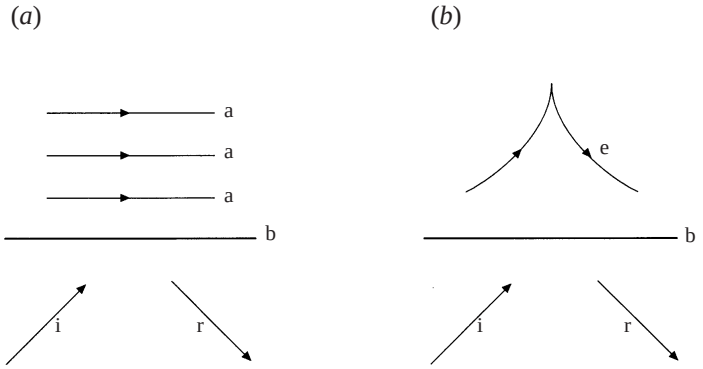

FIGURE 8. Incident wave i and reflected wave r at a boundary b producing total internal reflection. Above b the wave field is evanescent. (*a*) Averaged energy paths a; (*b*) typical exact energy path e, as in figures 4*c* and 5(*c*, *d*).

in one special case, the ordinary plane wave, the instantaneous and averaged energy paths are identical, being straight lines on which the energy travels at constant speed (at least on linear theory). This special case is of great importance, because far fields are locally planar. Thus the ideas in this paper are fully consistent with traditional analyses of energy flow in far fields, and only become interesting in, for example, near fields or edge waves. Furthermore, the results in this paper in no way imply that averaged energy fluxes are unimportant, even in near fields and edge waves. The averaged fluxes are of great importance, and global energy balances cannot do without them; but something is lost on taking the average, namely the origin and destination of the energy passing through a point. The ideas presented in this paper do not constitute a challenge to the method of averaging.

We have considered waves in semi-infinite half-space, but also of interest are bounded beams and propagation in waveguides. For example, consider a spinning acoustic field propagating inside a circular cylindrical duct. The way in which this field is diffracted at the end of the duct onto Keller cones implies that the acoustic energy in the duct propagates along piecewise linear helices (Chapman 1994); yet the averaged energy flow is everywhere parallel to the axis of the duct (Lighthill 1978, p. 420, equation 485). The conclusion seems inescapable that although a set of lines parallel to the axis of the duct leads to a correct mathematical formula for the total energy flow, these lines in themselves have no physical content, and only the piecewise linear helices can be related to measurable properties of the angular distribution of energy flow outside the duct. A similar argument shows that there are difficulties in using averaged paths for source localization. This is most vivid in optics: an observer seeing the sun and its reflection in a plane mirror finds that the mean energy flow is parallel to the mirror; but shadows point away from the sun and its image, not parallel to the mirror away from an 'average sun'. The same applies to reflection of sound which has come from a localized source. Again, the averaged paths appear to lack physical content.

Let us relate the above ideas to the simplest example of an edge wave, namely the spatially decaying steady evanescent wave produced by total internal reflection at a plane boundary. For such a wave, the traditional analysis of energy flow is as illustrated in figure 8(*a*): energy paths are parallel to the boundary, i.e. acoustic energy does not propagate away from the boundary into the medium above it. This analysis raises the difficulty of determining where the energy in the evanescent wave

comes from. Figure 8(*a*) suggests that at every height above the boundary there is an energy source far to the left; but there is no such source. Could the energy have arrived during an initial transient while the wave field was set up, simply to be stored thereafter? This is surely inconsistent with steady propagation of energy to the right. Or does the difficulty go away when the incident field is taken to be a bounded wave beam or a spherical wave? Our remarks in the previous paragraph make this seem unlikely.

The analysis in this paper resolves the above difficulty, which is seen to be a consequence of using energy paths averaged over a period. The exact energy paths, in figures 4(*c*) and 5(*c*, *d*), show that the evanescent wave is continuously supplied with energy from the incident wave, and continuously returns this energy to the reflected wave. The path taken by the energy varies periodically as shown in figure 4(*c*). Except for the discrete set of straight-line paths, every path has a cusp at the furthest point from the boundary, as shown in figure 8(*b*); at this cusp, the energy direction changes from upwards to downwards. An energy path arbitrarily close to a straight-line path penetrates arbitrarily far into the medium above the boundary, but must ultimately become cusped and return to the boundary. Thus our analysis leads us to reject the idea that an evanescent wave consists of a store of non-propagating energy. It is usually stated that the exponential decay of the field in an evanescent wave implies that there is no energy flow perpendicular to the boundary. In our analysis, the exponential decay is associated with exponential variation of ray-tube cross-sectional areas. Equation (2.49), for example, rewritten with $\mathrm{e}^{2(\theta_\mathrm{i}-\theta_{\mathrm{i}0})}$ on the right-hand side, may be shown to imply that the separation of neighbouring energy paths increases exponentially with distance from the boundary, up to a maximum at the cusps on the paths, and then decreases exponentially as the paths return to the boundary. Thus our analysis is consistent with the usual determination of the amplitude of a wave by applying conservation of energy to the energy flow in a ray tube.

The above discussion suggests that, in a wave field, averaged energy paths can give a misleading view of causality. Let us say that an energy path which traces back to an energy source is causal, and that any other energy path is acausal. The paths in figure 8(*b*) are causal, because the energy source is at the lower left, but the upper paths in figure 8(*a*) are acausal, because there is no energy source at the centre left: i.e. averaged paths have introduced the difficulty referred to in connection with source localization. Thus instantaneous energy paths provide superior insight into the classical problem of total internal reflection.

Similar considerations apply to an unsteady edge wave. For example, in an unstable flow which generates a temporally growing edge wave, the analysis in § 2 determines where the wave energy originates and where it goes. Figures 1 and 4 show that the more rapidly an edge wave grows in time, the greater is the tilt of the pressure contours away from the slowness direction $\boldsymbol{s}_\mathrm{i}$, and the greater is the asymmetry of a domain of influence about the slowness direction $\boldsymbol{s}_\mathrm{r}$.

The detailed application of the method of this paper to a varied set of problems in fluid dynamics would be of great interest. The method applies to any type of edge wave, for example a topographically trapped wave in the ocean, or a trapped water wave in a channel containing an obstacle. Possible applications are to the stability of fluid flow next to a compliant surface (Brazier-Smith & Scott 1984; Lingwood & Peake 1999); growth of waves in a boundary layer (Gaster 1962, 1965, 1968); instability in a spatially developing flow (Huerre & Monkewitz 1990); displacement of a sound beam on reflection from an elastic surface (Brekhovskikh 1980, p. 108; Brekhovskikh & Godin 1992, p. 39); scattering of sound by a shear layer (Miles

1958; Jones & Morgan 1974; Jones 1977); and jet noise (Tam 1971, 1972; Troutt & McLaughlin 1982; Tam & Burton 1984*a*, *b*). A classical problem that could be looked at afresh is that of energy flow near a caustic, e.g. near the sonic radius in a rotating sound field (Prentice 1993); the well-known phase change of $\frac{1}{2}\pi$ in the pressure field on a ray gives no clue to the delay on an energy path. Indeed, the results of this paper suggest that, near a caustic, energy is continuously flowing deep into the exponentially decaying zone and later re-emerging from it at some distance from the point of entry. Similarly, it would be possible to determine the energy paths in the Fresnel zone at a shadow boundary; an intriguing question is whether the increasing width of such a zone is related to the curved shape, near the origin, of the domain of influence shown in figure 4(*c*). In all these examples, one may expect the calculation of the energy paths to reveal hitherto unsuspected structure in the wave field.

This work owes much to discussions with F. J. Fahy at the Institute of Sound and Vibration Research, University of Southampton, on source detection in acoustics, and to a study of J. Lighthill's papers on the energy velocity of fluid and elastic waves in the cochlea.

REFERENCES

Boulanger, Ph. & Hayes, M. 1993 *Bivectors and Waves in Mechanics and Optics*. Chapman & Hall.

Brazier-Smith, P. R. & Scott, J. F. 1984 Stability of fluid flow in the presence of a compliant surface. *Wave Motion* **6**, 547–560.

Brekhovskikh, L. M. 1980 *Waves in Layered Media*, 2nd Edn. Academic.

Brekhovskikh, L. M. & Godin, O. A. 1992 *Acoustics of Layered Media. II. Point Sources and Bounded Beams*. Springer.

Buchen, P. W. 1971 Plane waves in linear viscoelastic media. *Geophys. J. R. Astron. Soc.* **23**, 531–542.

Buchwald, V. T. 1972 Energy and energy flux in planetary waves. *Proc. R. Soc. Lond.* A **328**, 37–48.

Chapman, C. J. 1994 Sound radiation from a cylindrical duct. Part 1. Ray structure of the duct modes and of the external field. *J. Fluid Mech.* **281**, 293–311.

Gaster, M. 1962 A note on the relation between temporally-increasing and spatially-increasing disturbances in hydrodynamic stability. *J. Fluid Mech.* **14**, 222–224.

Gaster. M. 1965 On the generation of spatially growing waves in a boundary layer. *J. Fluid Mech.* **22**, 433–441.

Gaster, M. 1968 Growth of disturbances in both space and time. *Phys. Fluids* **11**, 723–727.

Gill, A. E. 1982 *Atmosphere-Ocean Dynamics*. Academic.

Hayes, M. 1977 A note on group velocity. *Proc. R. Soc. Lond.* A **354**, 533–535.

Hayes, M. 1980 Energy flux for trains of inhomogeneous plane waves. *Proc. R. Soc. Lond.* A **370**, 417–429.

Huerre, P. & Monkewitz, P. A. 1990 Local and global instabilities in spatially developing flows. *Ann. Rev. Fluid Mech.* **22**, 473–537.

Jones, D. S. 1977 The scattering of sound by a simple shear layer. *Phil. Trans. R. Soc. Lond.* A **284**, 287–328.

Jones, D. S. & Morgan, J. D. 1974 A linear model of a finite amplitude Helmholtz instability. *Proc. R. Soc. Lond.* A **338**, 17–41.

Lighthill, M. J. 1960 Studies on magneto-hydrodynamic waves and other anisotropic wave motions. *Phil. Trans. R. Soc. Lond.* A **252**, 397–430.

Lighthill, M. J. 1965 Group velocity. *J. Inst. Maths Applics.* **1**, 1–28.

Lighthill, J. 1978 *Waves in Fluids*. Cambridge University Press.

Lighthill, J. 1981 Energy flow in the cochlea. *J. Fluid Mech.* **106**, 149–213.

Lingwood, R. J. & Peake, N. 1999 On the causal behaviour of flow over an elastic wall. *J. Fluid Mech.* **396**, 319–344.

Longuet-Higgins, M. S. 1964 On group velocity and energy flux in planetary wave motions. *Deep-Sea Res.* **11**, 35–42.

Luyten, J. R. 1973 Topographic Rossby waves: a cautionary tale. *Mém. Soc. R. Sci. Liège* 6^{e} série **6**, 167–177.

Miles, J. W. 1958 On the disturbed motion of a plane vortex sheet. *J. Fluid Mech.* **4**, 538–552.

Noda, A. 1986 A general relationship between group velocity and fluxes quadratic in wave amplitude. *J. Met. Soc. Jap.* **64**, 319–327.

Pedlosky, J. 1987 *Geophysical Fluid Dynamics*, 2nd Edn. Springer.

Prentice, P. R. 1993 Energy transport in rotating sound fields. *Proc. R. Soc. Lond.* A **441**, 83–96.

Scott, N. H. 1995 Inhomogeneous plane waves in compressible viscous fluids. *Wave Motion* **22**, 335–347.

Tam, C. K. W. 1971 Directional acoustic radiation from a supersonic jet generated by shear layer instability. *J. Fluid Mech.* **46**, 757–768.

Tam, C. K. W. 1972 On the noise of a nearly ideally expanded supersonic jet. *J. Fluid Mech.* **51**, 69–95.

Tam, C. K. W. & Burton, D. E. 1984*a* Sound generated by instability waves of supersonic flows. Part 1. Two-dimensional mixing layers. *J. Fluid Mech.* **138**, 249–271.

Tam, C. K. W. & Burton, D. E. 1984*b* Sound generated by instability waves of supersonic flows. Part 2. Axisymmetric jets. *J. Fluid Mech.* **138**, 273–295.

Thomson, R. E. 1973 The energy and energy flux of planetary waves in an ocean of variable depth. *Geophys. Fluid Dyn.* **5**, 385–399.

Troutt, T. R. & McLaughlin, D. K. 1982 Experiments on the flow and acoustic properties of a moderate-Reynolds-number supersonic jet. *J. Fluid Mech.* **116**, 123–156.